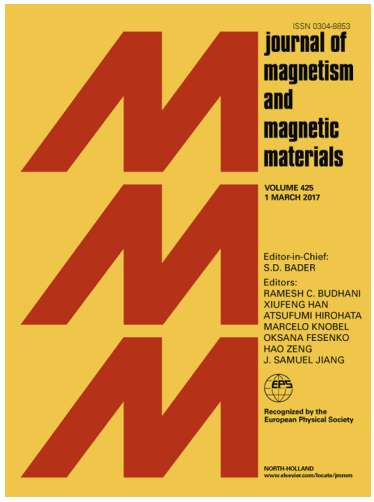

Magnetic ordering in the nano-laminar ternary Mn_2AlB_2 using neutron and X - ray diffraction

D. Potashnikov, E.N. Caspi, A. Pesach, A. Hoser, S. Kota, L. Verger, M.W. Barsoum, I. Felner, A. Keren, O. Rivin

PII: S0304-8853(18)32175-9
DOI: https://doi.org/10.1016/j.jmmm.2018.09.078
Reference: MAGMA 64360

To appear in: *Journal of Magnetism and Magnetic Materials*

Received Date: 11 July 2018
Revised Date: 30 August 2018
Accepted Date: 22 September 2018

Please cite this article as: D. Potashnikov, E.N. Caspi, A. Pesach, A. Hoser, S. Kota, L. Verger, M.W. Barsoum, I. Felner, A. Keren, O. Rivin, Magnetic ordering in the nano-laminar ternary Mn_2AlB_2 using neutron and X - ray diffraction, *Journal of Magnetism and Magnetic Materials* (2018), doi: https://doi.org/10.1016/j.jmmm.2018.09.078

Magnetic ordering in the nano-laminar ternary Mn_2AlB_2 using neutron and X - ray diffraction

D. Potashnikov,[a,b] E.N. Caspi,[c,d] A. Pesach,[c] A. Hoser,[e] S. Kota,[d] L. Verger,[d] M. W. Barsoum,[d] I. Felner,[f] A. Keren[a] and O. Rivin[c,e]

Sep 2018

[a] *Faculty of Physics, Technion - Israeli Institute of Technology, Haifa 32000, Israel*

[b] *Israel Atomic Energy Commission, P.O. Box 7061, Tel-Aviv 61070, Israel*

[c] *Department of Physics, Nuclear Research Centre-Negev, P.O. Box 9001, Beer Sheva 84190, Israel*

[d] *Department of Materials Science and Engineering, Drexel University, Philadelphia, PA, United states*

[e] *Helmholtz-Zentrum Berlin fur Materialen und Energie, Berlin, Germany*

[f] *Racah Institute of Physics, Hebrew University of Jerusalem, 91904 Jerusalem, Israel*

Abstract

The nano-laminar ceramic Mn_2AlB_2 belongs to the orthorhombic M_2AlB_2 system (M = Cr, Fe, Mn), in which Fe_2AlB_2 was shown to be ferromagnetic near room temperature. Herein, the magnetic state of $Mn_2Al^{11}B_2$ is investigated using magnetization, in the 5 to 360 K temperature range, X-ray diffraction in the 300 to 800 K range and neutron diffraction in the 1.6 to 300 K range. From the totality of our results we conclude that below ~ 390 K Mn_2AlB_2 becomes a canted antiferromagnet. The crystallographic unit cell is doubled along the c axis (i.e. a propagation vector of 0,0,1/2) and the ordered Mn magnetic moments are oriented either along the a or the b axes, with a magnetic moment reaching 0.71(2) μ_B per Mn atom at 1.6 K. This magnetic structure is in excellent agreement with, and contributes to the validity of the recently reported theoretical calculations for the $(Fe_{1-x}Mn_x)_2AlB_2$ system.

Keywords: antiferromagnetism; laminar structures; neutron diffraction; canting

I. Introduction

The magnetic properties of boride compounds have attracted scientific attention over the years. For example, $Nd_2Fe_{14}B$ was found [1] to simultaneously exhibit high magnetic anisotropy and ordered magnetic moment. The binary transition metal (M) borides, M_nB_m, were shown [2–4], to order magnetically at relatively high temperatures (~ 600 K). While Fe_2B was shown [3] to be ferromagnetic

(FM), MnB_2 was shown [5] to undergo two magnetic transitions. The first led to an antiferromagnetic (AFM) structure and the second generated a canted AFM structure.

In recent years, interest was spurred in the ternary M_2AlB_2 with M = Fe, Mn, Cr [6]. These materials crystallize in an orthorhombic structure (Cmmm space group), with a nano-laminated layout (Fig. 1, inset) [7,8]. The 2D slabs of M_2B_2 atoms form a "zigzag" type chain arrangement intertwined with layers of Al. Fe_2AlB_2 was found to become FM near room temperature (RT) [9], and showed promising magnetocaloric (MC) properties [10,11]. The macroscopic magnetic properties of the $(Fe_{1-x}Mn_x)_2AlB_2$ system and Cr_2AlB_2 were investigated using Mössbauer spectroscopy and magnetization measurements [8]. It was found that the admixture of Mn into Fe_2AlB_2 decreases the ordered magnetic moments and ordering temperature, and also generated a rapid change in the lattice parameters. On the other hand, the magnetic properties of Mn_2AlB_2 and Cr_2AlB_2 remained unclear. Another study of the $(Fe_{1-x}Mn_x)_2AlB_2$ system reported [12] that the x = 0.25 compound exhibits a spin glass type behavior below ~ 50 K. These were attributed to the competing FM and AFM exchange interactions contributed by the Fe and Mn atoms respectively. These exchange interactions were later supported by a theoretical study [13] of the $(Fe_{1-x}Mn_x)_2AlB_2$ system, which found that Fe_2AlB_2 and Mn_2AlB_2 are magnetically ordered at low temperature, with a FM and AFM structures, respectively. The magnetic moments were reported to be oriented within the a-b plane, and the crystallographic unit cell is doubled along the c axis within the AFM Mn_2AlB_2 structure.

In the present work, we synthesized the $Mn_2Al^{11}B_2$ compound using isotopic ^{11}B in order to investigate the magnetic structure of Mn_2AlB_2 using neutron powder diffraction (NPD). The thermal expansion of the lattice parameters above RT is supplemented by X-ray powder diffraction (XRD). Our primary aim is to determine whether Mn_2AlB_2 is AFM, thus validating the previously suggested [12,13] nature of the exchange interaction of Mn within M_2AlB_2. We hope that such AFM interactions may enable future tuning of desirable magnetic properties within M_2AlB_2, including the MC effect.

II. Experimental details

Manganese (99.3 % pure, -325 mesh), aluminum (99.5 %, 7-15 μm particle size), and boron (98 %, -325 mesh) powders from Alfa Aesar were mixed in an atomic ratio of 2:1.5:2, respectively, in a polyethylene jar with zirconia milling balls on a tumble ball mill for 24 h for the high-temperature XRD sample (henceforth referred to as sample A). The NPD powders included isotopically pure ^{11}B powders (99.5 % pure, particle size < 44 μm; henceforth referred to as sample B). The powders were subsequently cold-pressed into pellets with loads corresponding to a stress of 100 MPa in a steel die,

and heated, under flowing Ar, at a rate of 4 K/min to a temperature of 1293 K. This temperature was maintained for 15 h before passive furnace cooling. The porous billet, showing signs of a large volume expansion, was crushed into fine powders in an agate mortar and pestle for further characterization.

XRD was performed at RT with a Bruker D8 – Advance diffractometer, using CuKα radiation at the Nuclear Research Centre – Negev. A powder portion from sample B was placed on a silicon wafer and measured in a Bragg – Brentano type diffraction geometry. An angular range of 10° to 100° was covered in steps of 0.01°. Data was analyzed by the Rietveld refinement method, using the FULLPROF code [14].

High temperature XRD patterns were acquired on a powder of sample A using a Rigaku SmartLab powder diffractometer in Bragg-Brentano geometry in the 10-155º 2-theta range using 0.01º step size and a speed of 3º/min. XRD patterns were acquired at RT and every 100 K in the 300-800 K temperature range, on heating and cooling, using a heating stage (Antonn Paar DHS1100) with a N_2 gas atmosphere and hemispherical graphite dome. Lattice constants at each temperature were calculated by the Le Bail refinement method using Jana software [15].

Magnetization (M) measurements, as function of T, were carried out on powder portions from sample B using a Quantum-Design SQUID magnetometer at the Hebrew University in Jerusalem. M as a function of T was obtained using applied magnetic fields of 85 Oe and 250 Oe, in the temperature ranges of 5 to 300 K and 280 to 360 K, respectively. Field dependent M, in the 0 to 50 kOe range, was obtained on powder portions from sample B using a Cryogenic S700 SQUID magnetometer at the Technion – Israel Institute of Technology. The measurements were performed at temperatures of 5, 25, 50, 100, 200 and 290 K.

NPD was performed on sample B at the E6 high flux neutron diffractometer at the Helmholtz – Zentrum in Berlin. The measurements were performed at 1.6, 5, 10, 25, 50, 65, 100, 200 and 298 K. An incident neutron wavelength of 2.43(1) Å was obtained using a focusing pyrolytic graphite monochromator. Four grams of powder sample B were loaded into a 6 mm in diameter cylindrical vanadium holder. Data was analyzed by the Rietveld refinement method, using the FULLPROF code [14].

III. Results and analysis

IIIa. X-ray powder diffraction

The majority of reflections in the observed XRD pattern at RT (Fig. 1, symbols) of the studied sample is consistent with an orthorhombic structure having the lattice parameters (LPs) a ~ 2.92, b ~ 11.07, and c ~ 2.90 Å. These results are in good agreement with previously reported LPs of Mn_2AlB_2 [6]. Additional reflections were identified to belong to the $MnAl_4$ [16], $MnAl_6$ [17], and Al_2O_3 [18] impurity phases. Therefore, a 4-phase model was refined to the data using the Rietveld refinement method. The refined profile (Fig. 1, solid black line) was generated assuming the major phase, Mn_2AlB_2, having the orthorhombic *Cmmm* space group, with the Mn, Al and B atoms occupying the 4j, 2a and 4i sites, respectively. Additional impurity phases $MnAl_4$ (*P6/3m*), $MnAl_6$ (*Cmcm*) and Al_2O_3 (*R-3c*) were also used in the model. A summary of the structural refined parameters is given in Table I. Attempts to dissolve the intermetallic impurities in dilute hydrochloric acid, as previously demonstrated for Fe_2AlB_2 [8,10,11], were unsuccessful since the Mn_2AlB_2 was also quite susceptible to dissolution.

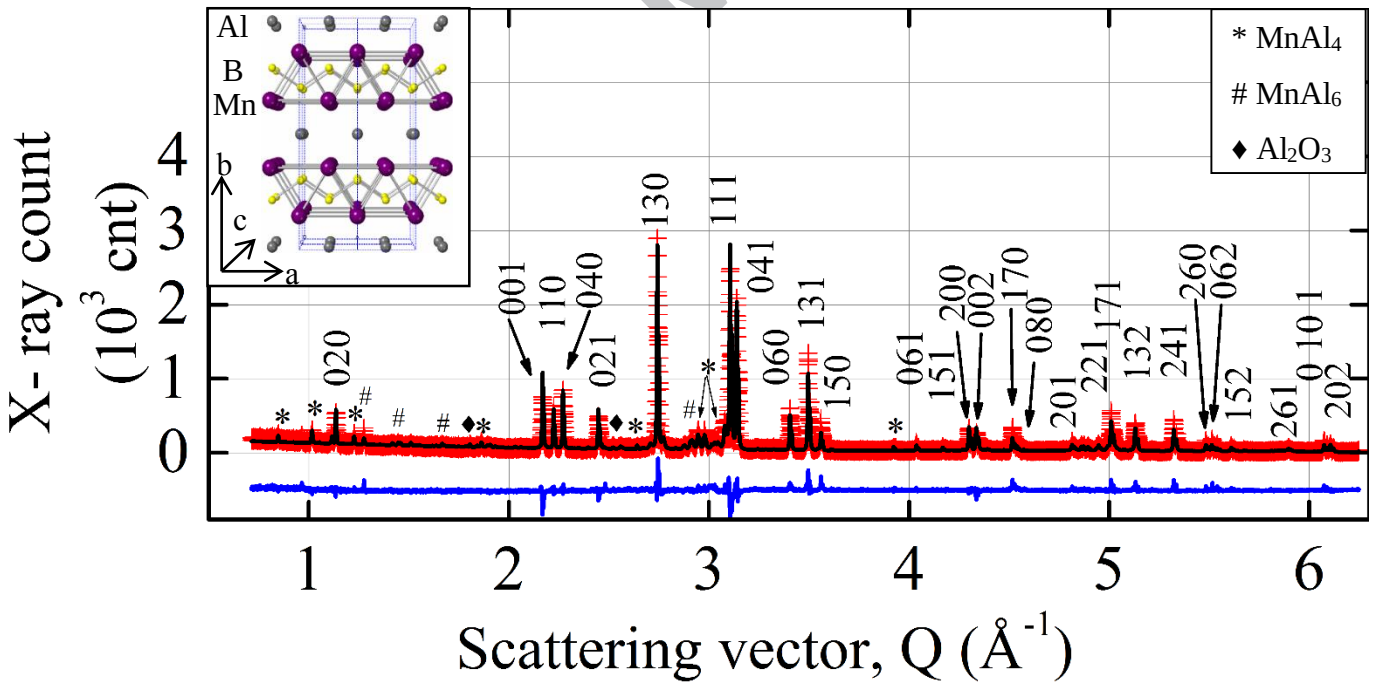

Fig. 1. XRD pattern of Mn_2AlB_2 powders at RT (red crosses), the Rietveld refined profile (black line). The difference is given by the blue line at the bottom. Some reflections originating from Mn_2AlB_2 are denoted by their Miller indices, reflections belonging to impurity phases are marked with * ($MnAl_4$), # ($MnAl_6$) and ♦ (Al_2O_3). Inset highlights the laminated structure of M_2AlB_2.

Table I. Room temperature XRD and NPD Rietveld refined lattice parameters, the Mn (y_{4j}) and B (y_{4i}) atomic position in Mn_2AlB_2 (sample B) and relative amount of each phase, obtained herein (top 5 rows). Numbers in parentheses are statistical uncertainties of the last significant digits obtained from the refinement process. Previous XRD work is shown in bottom 3 rows.

Method	Phase	a(Å)	b(Å)	c(Å)	y_{4j}	y_{4i}	wt %
XRD	Mn_2AlB_2	2.92267(3)	11.0715(1)	2.89776(3)	0.3547(1)	0.2029(8)	68.3(5)
	$MnAl_4$	28.3496(8)	---	12.3790(6)	---	---	23.3(4)
	$MnAl_6$	7.5505(8)	6.5071(8)	8.8703*	---	---	6.7(3)
	Al_2O_3	4.7592(1)	---	12.9937(6)	---	---	1.8(2)
NPD	Mn_2AlB_2	2.9166(6)	11.048(3)	2.8930(6)	0.3556(3)	0.2061(3)	---
XRD	Mn_2AlB_2 [8]	2.936(5)	11.12(1)	2.912(8)	---	---	†
	Mn_2AlB_2 [7]	2.9180(4)	11.038(2)	2.8932(5)	0.35509(5)	0.2063(3)	‡
	Mn_2AlB_2 [19]	2.92	11.08	2.89	0.355	0.209	‡

--- Not considered.
* No convergence reached and fixed at its literature value [17].
† Contains Mn_3Al_{10} impurities. Quantity of impurity phase not mentioned.
‡ Contains $MnAl_6$ and AlB_2 impurities. Quantity of impurity phase not mentioned.

IIIb. Magnetization

The M obtained by cooling under an applied magnetic field (M_{FC}) of 85 Oe, and that obtained by cooling under a near zero field (M_{ZFC}), depart at ~ 340 K, and exhibit a mild (and close to linear) increase and decrease, respectively of ~30% and 50%, as the temperature is lowered from 298 to 1.6 K (Fig. 2(a)). This behavior is consistent with the presence of a low anisotropy ordered magnetic structure [20]. This conclusion is further supported by field dependent magnetization measurements (not shown) that show no hysteresis loops, indicating that similar to Fe_2AlB_2, Mn_2AlB_2 is also a soft magnet [11]. Although paramagnetic [21–24], the impurity phases listed in Table I., contribute to the magnitudes of M_{FC} and M_{ZFC}, leading to the overestimated observed values. On the other hand, significant variations in the temperature derivatives (dM_{FC}/dT and dM_{ZFC}/dT, Fig. 2(b)), serve as good indicators [25,26] for T's at which the M exhibits a rapid change (i.e. a magnetic event). Three such magnetic events are found at 25(1), 34(1) and 220(10) K.

At T's higher than 25 K, M as a function of externally applied magnetic field (H_{ext}, Fig. 2(c), symbols) exhibits a spontaneous [20,27] ferromagnetic (or ferrimagnetic) type magnetization increase (M_{sp}) up to ~18 kOe, followed by an almost linear increase (18 kOe < H_{ext}) that can be attributed to

field induced paramagnetism of an ordered structure. Below 50 K, the paramagnetic increase becomes concave and exhibits a Brillouin [28] type increase at 5 K. To properly account for the paramagnetic contribution to M by the ordered magnetic structure and the impurities (see Appendix A for details), a susceptibility term, proportional to H_{ext}, and a Brillouin type [28] term are considered (Eq. 1). We assume that the impurities' paramagnetic contribution originates from Mn ions alone (Table I), in which the orbital contribution to the magnetic moment is quenched [28] by the crystalline electric field.

$$M(H_{ext},T) = M_{sp}(T) + \chi(T)H_{ext} + n_i N_A g S \mu_B B_S(H_{ext},T) \quad (1)$$

$\chi(T)$ is the susceptibility of the ordered magnetic structure, n_i is the number of Mn moles within the sample, N_A is Avogadro's constant, $g = 2$ is the gyromagnetic ratio, S is the Mn equivalent spin, μ_B is Bohr magneton and $B_S(y) \equiv (2S + 1)/2S \coth(\{2S + 1\}y/2S) - \coth(y/2S)/2S$ is the Brillouin function, $y \equiv gS\mu_B H_{ext}/k_B T$, k_B is Boltzmann's constant and T is the sample temperature. M_{sp} at each temperature (Table A.I) is obtained by fitting Eq. 1 to the observed M (Fig. 2(c), lines) for 18 kOe < H_{ext}. Below 18 kOe, the observed M are dominated by the alignment of magnetic domains, under the action of H_{ext}, which leads to M_{sp}.

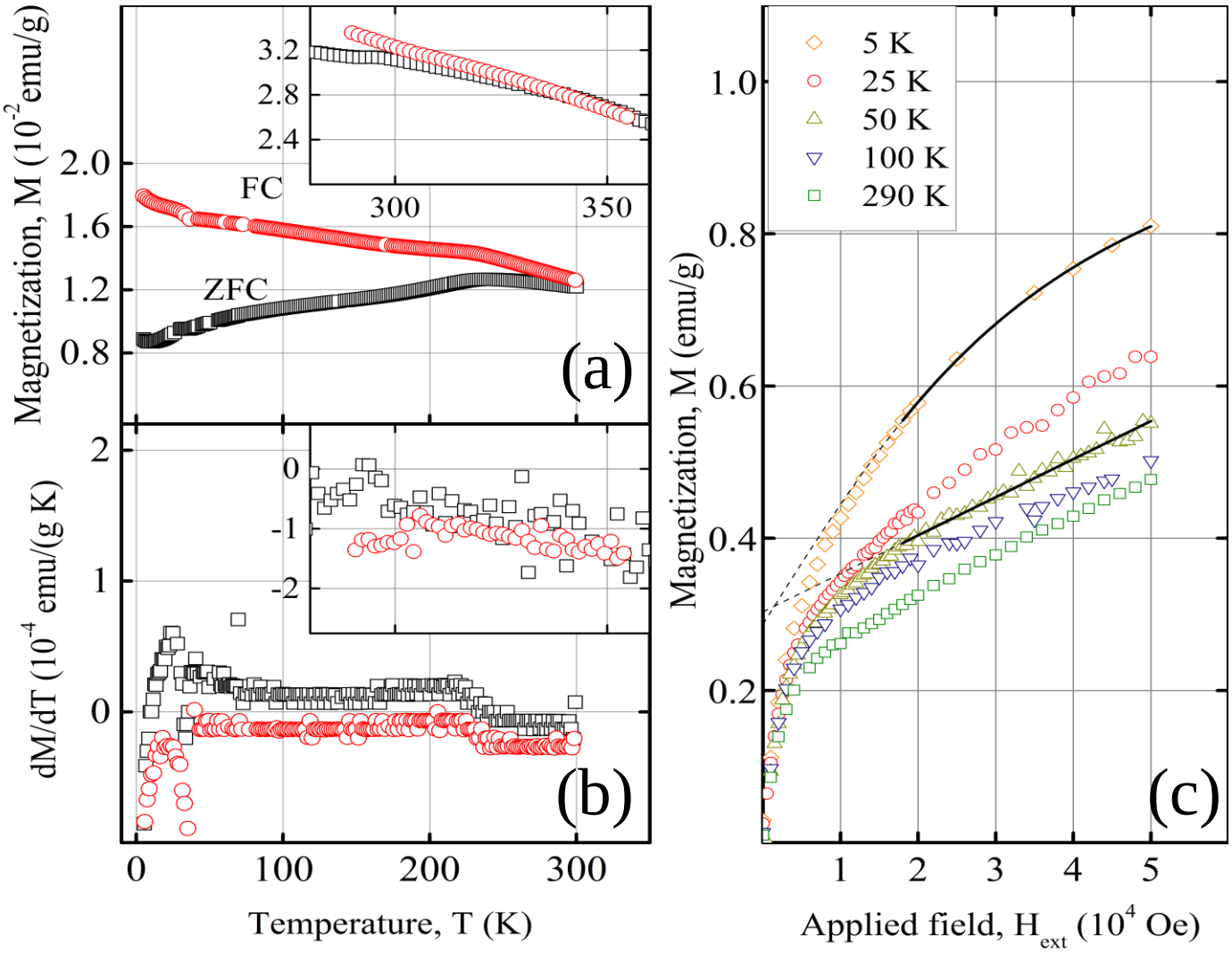

Fig. 2. Magnetization (M) of sample B: (a) M as function of T after cooling under a (near) zero externally applied magnetic field (ZFC, squares) and after cooling under an applied field of 85 Oe (FC, circles). (b) dM/dT for the FC (85 Oe) and ZFC conditions. Insets presents observed M values obtained under an applied field of 250 Oe. (c) M as function of externally applied field (symbols) at different temperatures. The fit of Eq. 1 (solid lines) to the observed M values, for 18 kOe < H_{ext}, at 5 and 50 K is also presented (solid line), with the extrapolation to lower H_{ext} values (dashed).

IIIc. Neutron powder diffraction

The majority of reflections in the observed NPD pattern from sample B (Fig. 3(a)) are consistent with orthorhombic structure having LPs a ~ 2.92, b ~ 11.05, and c ~ 2.89 Å - in good agreement with the XRD results (Table I) , within the limits of statistical uncertainty (Table I.) and systematic uncertainty (Sec IIId). Additional reflections were found to be consistent with the $MnAl_6$

impurity phase, however due to the low neutron count of these reflections, the structural parameters of $MnAl_6$ were not refined within the NPD. However, adding or neglecting the $MnAl_6$ to the refinement process did not lead to any change in the refined Mn_2AlB_2 parameters. Hence, the refinement of the observed RT profile consisted of a 1-phase model. The structural parameters of Mn_2AlB_2 obtained in the XRD analysis (Fig. 1) served as the initial refinement conditions. The refined NPD parameters are in good agreement with the XRD results (Table I.). Upon cooling below RT down to 200 K, the a and b lattice parameters exhibit an anomalous increase (Fig. 4(a) and 4(b), solid symbols) that is consistent with magnetostriction, driven by magnetic ordering at a higher temperature.

Indeed, upon cooling, an increase in the neutron count of a reflection, with a scattering vector of Q = 1.08 $Å^{-1}$, is observed (Fig. 3 insets). This reflection, together with two new reflections that appear upon cooling (Fig. 3(b)), are consistent with a magnetic structure that originates from the Mn_2AlB_2 phase, with a magnetic unit cell that doubles the crystallographic unit cell along the c axis (propagation vector k = 0,0,1/2). The refined magnetic structure is then applied to the RT measurements, and fits the reflection at Q = 1.08 $Å^{-1}$ (Fig. 3(a) inset), showing that Mn_2AlB_2 is magnetically ordered at RT.

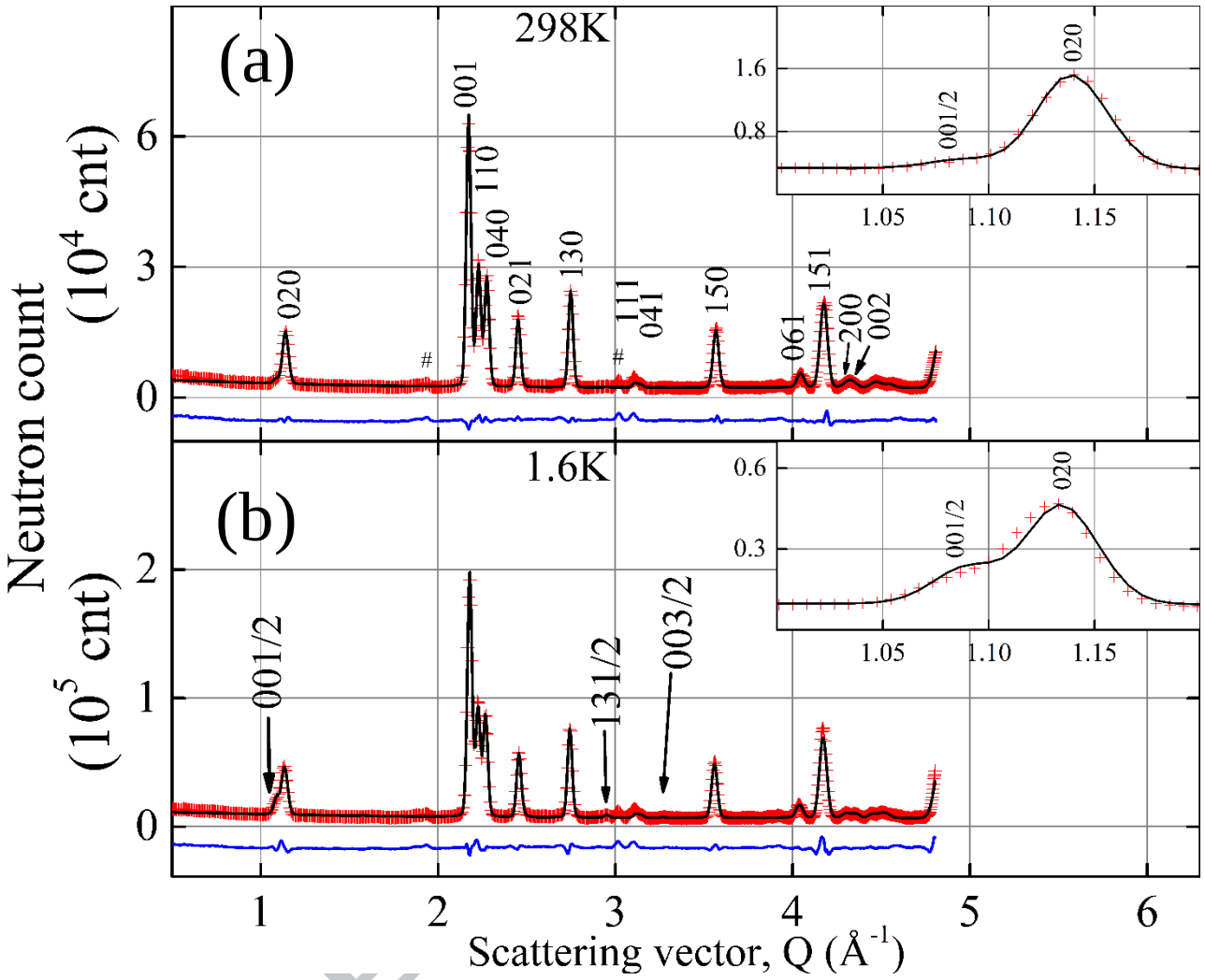

Fig. 3.The observed neutron powder diffraction profile of Mn_2AlB_2 (red crosses) at, a) room temperature and, b) at 1.6 K. The Rietveld refined profile (black line) and the difference between the observed and refined profile (blue line at the bottom) are also shown. Some reflections originating from the a) crystallographic and, (b) magnetic structures are denoted by their Miller indices and fractional Miller indices, respectively. Reflections originating from $MnAl_6$ impurity are denoted by #. Insets present the crystallographic (0,2,0) and the magnetic (0,0,1/2) reflections.

Symmetry analysis of the irreducible representations of the propagation vector group was performed using the BasIreps [29] routine within the FP package. Assuming Mn_2AlB_2 remains orthorhombic, 6 configurations of the ordered Mn magnetic moments (μ_{AFM}) corresponding to the irreducible representations of the propagation vector group, are possible. The refined profile, calculated for each configuration using FP, is consistent with the observed profile (Fig. 3(b)) for 2

configurations, termed I and II, according to which the μ_{AFM} are oriented either along the a or b (Fig. 4(b) inset) crystal axes, respectively.

The reported uncertainty of the refined lattice parameters at different temperatures (see Table B.I in Appendix B) is dominated by the statistical uncertainty in the observed neutron count and is reported by the FP convergence algorithm. On the other hand, the uncertainty in the refined μ_{AFM} (solid symbols in Fig. 4(c)) is combined from the statistical uncertainty and the codependence between μ_{AFM} and the instrumental parameters of E6. This codependence is obtained using a process similar to that described in Table A.I. The difference in the refined μ_{AFM} values, due to configurations I and II (Table B.II) also contributes to the reported μ_{AFM} uncertainty.

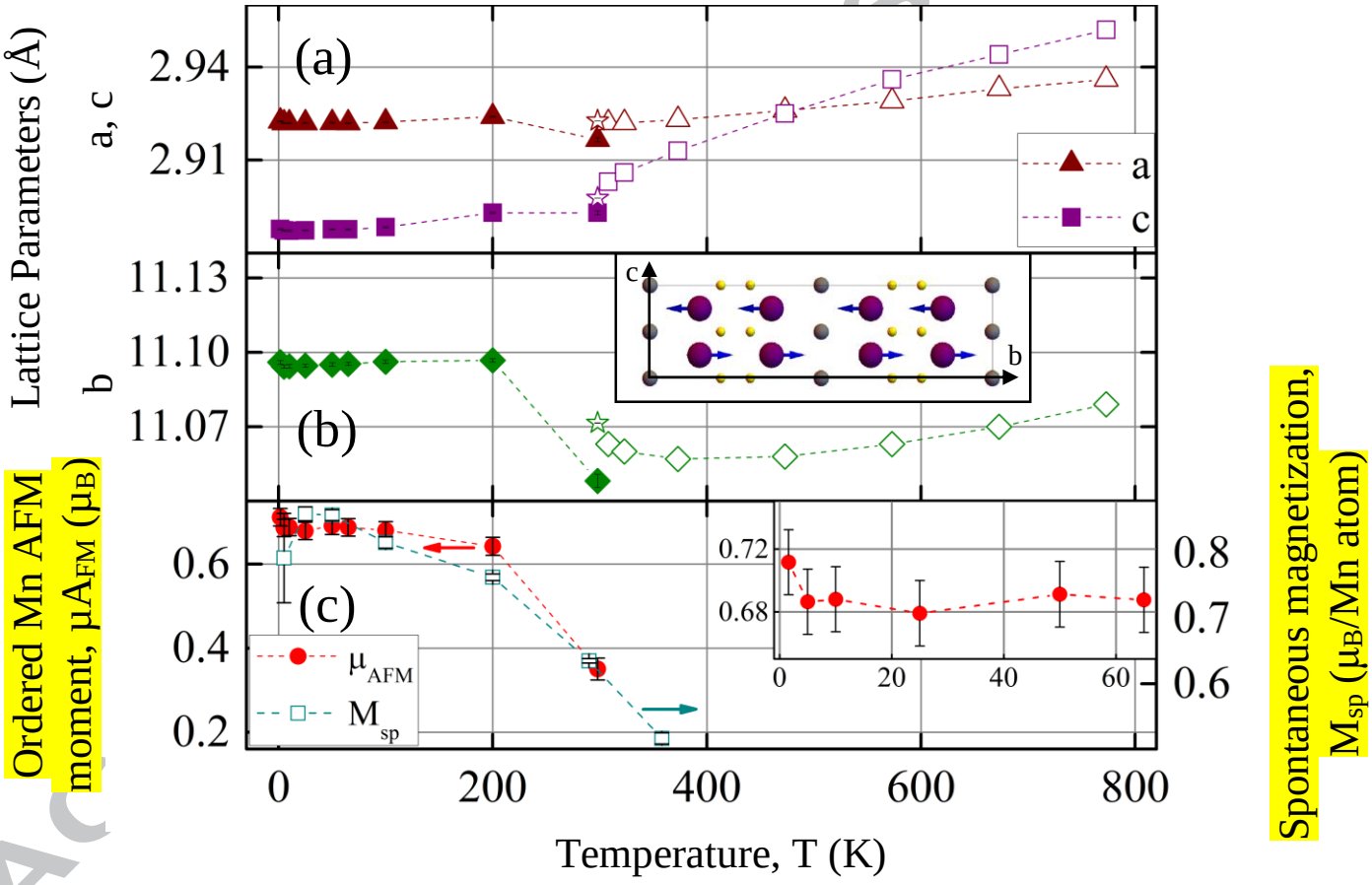

Fig. 4. Temperature dependencies of, a), a and c and, b) b-LPs refined unit cell lattice parameters obtained from NPD (full symbols – shifted by +0.2%, see text) and high T XRD (open symbols) of Mn_2AlB_2. The star indicates the RT XRD refined lattice parameters. Inset is an illustration of the magnetic structure according to configuration II. c) Ordered Mn AFM moment (μ_{AFM}, solid symbols) and spontaneous magnetization (M_{sp}, open symbols) obtained from NPD, and macroscopic

magnetization measurements, respectively. Inset zooms in on the AFM component at low T. Dotted lines are guides to the eye.

IIId. High temperature X-ray powder diffraction

The temperature evolution of the LPs in 300 to 800 K temperature range (Fig. 4(a) and 4(b)) shows that, the a and c LPs increase more or less monotonically with increasing T. The b LP, on the other hand, drops significantly around RT (Fig. 4(b)), before expanding significantly again, resulting in a minimum in the b LP value at ~ 400 K.

Fig. 4(c) plots the magnetic moments on the Mn atoms as a function of T. From the fact that the drop in μ coincides with the drop in b LP, it is reasonable to conclude that they are related and that the onset of magnetic ordering results in magnetostriction. Note that the a and c lattice parameters appear to coincide at ~ 470 K, and a tetragonal-like symmetry may be considered. However, since the a and c LPs depart in value upon heating or cooling from that temperature, we conclude that a tetragonal structure is unstable.

When the RT XRD and RT NPD LPs, measured on powders from sample B, are compared, (Table I) the latter are systematically shifted to lower values by ~ 0.2% for the a and c (Fig. 4 (a)) and the b (Fig. 4 (b)) LPs. This shift likely originates from a systematic calibration uncertainty in either the XRD or the E6 neutron diffractometer or the combination of the two. When comparing the XRD LPs determined at RT from sample B measurement (Fig. 4 (a) and (b) – stars) with those determined at HT from sample A measurement (Fig. 4 (a) and (b) – open symbols), excellent agreement is obtained. Moreover, the E6 incident wavelength uncertainty (~0.4%) may account for this shift alone. This systematic uncertainty is significantly lower than the anomalous expansion upon cooling observed for the b LP, and does not contradict the observed magnetostriction.

IV. Discussion

The NPD analysis shows that Mn_2AlB_2 is AFM from 1.6 K to RT (Fig. 3). However, an AFM structure is inconsistent with M_{sp} (Fig. 2(c)). The 5 K M_{sp} value (Table A.I) is equivalent to a ferromagnetic moment of $7.9(7)\times10^{-3}$ μ_B per Mn atom within Mn_2AlB_2, and is far below the NPD sensitivity limit. Because the identified impurities were previously reported to be paramagnetic [21–24], and M_{sp} exhibits an increase between 290 and 200 K (Fig. 4(c), open symbols) followed by a plateau down to 5 K, in agreement with the temperature evolution exhibited by the NPD based μ_{AFM}

(solid symbols), we propose that both are components of the *same* ordered magnetic moment that originates from Mn_2AlB_2. Said otherwise, we postulate that M_{sp} originates from a small canting of the ordered AFM Mn magnetic moments, thus generating a small net ferromagnetic moment. Using the 5 K μ_{AFM} and M_{sp} values we obtain a canting angle of ~ 0.6°. We note in passing that canted AFM structures, with low temperature canting angles of less than a degree, were previously reported [27].

While no NPD data is available above RT, field dependent magnetization at 358 K (Fig. 4(c)) has showed that the (canted) FM component is present at this temperature. If both originate from the same ordered moment, the magnetic ordering temperature (T_C) would be higher than 358 K. If the anomalous temperature evolution of the b LP below 390 K (Fig. 4(b)) is indeed the result of magnetostriction, then we speculate that T_C is higher by a few degrees. In addition to T_C, below 5 K both μ_{AFM} (Fig. 4(c) inset) and the lattice parameters (Fig. 4(b)) exhibit a simultaneous increase. Interestingly, a large susceptibility increase has been previously reported at this temperature [8]. We also note that, the observed M (Fig. 2(c)) is also consistent with a low magnetic anisotropy of the magnetic structure of Mn_2AlB_2.

Because only a small number of magnetic reflections are observed (Fig. 3), the magnetic agreement factor, $R_{m,f}$, provided by the refinement process, is large (Table B.II). Thus, while seemingly configuration I (Sec IIIc) provides better agreement with the observed results (Table B.II), we argue that configuration II cannot be excluded based on the experimental precision in the present work, and both configurations are consistent. On the other hand, our group theoretical analysis predicts that the magnetic structure contains either configuration I or configuration II but not a superposition of both.

V. Conclusions

Using neutron powder diffraction, Mn_2AlB_2 is determined to be antiferromagnetic from 1.6 K and up to RT (Fig. 3). The crystallographic unit cell is doubled along the c axis and the ordered Mn magnetic moments are oriented either along the a or along the b axes. At 1.6 K, the size of the ordered Mn magnetic moment is 0.71(2) μ_B.

The above mentioned magnetic structure, in general, and the spins configuration, in particular, is in excellent agreement with recent theoretical calculations [13]. Hence, the results in the present work contribute to the validity of the latter.

Magnetization experiments reveal the presence of a small ferromagnetic component at 290 K and down to 5 K (Fig. 2(c)). Since the identified impurities are paramagnetic (Table I) and the temperature evolution of the FM component is similar to that of the antiferromagnetic structure (Fig.

4(c)), we propose that it originates from canting of the Mn_2AlB_2 antiferromagnetic structure. The 5 K canting angle is calculated to be ~ 0.6°.

The b lattice parameter exhibits an increase as the temperature is decreased below ~ 390, and down to ~ 200 K (Fig. 4(b)). At ~ 290 K, the a lattice parameter exhibits similar behavior, and both are accompanied by a steep increase in the magnitude of the ordered Mn magnetic moment (Fig. 4(c)). We suggest that these changes originate from magnetostriction.

The magnetic ordering temperature of Mn_2AlB_2 is higher than 358 K, at which a ferromagnetic component is found. We suggest that Mn_2AlB_2 undergoes magnetic ordering just above 390 K, where the anomalous lattice parameters expansion is observed. The wide temperature range between the Fe_2AlB_2 transition temperature (~ 285 K), and the Mn_2AlB_2 transition (~ 390 K), as well as the rich magnetic structure of Mn_2AlB_2, that contains both AFM and FM components, holds much promise for tunability of application relevant MC properties in the $(Fe_{1-x}Mn_x)_2AlB_2$ solid solutions and maybe for other MAB phases as well.

Acknowledgements

We wish to thank Dvir Fadel for his assistance in obtaining the XRD patterns shown in Fig. 1. We also thank Thierry Ouisse and Herve Roussel from the Université Grenoble-Alpes, CNRS, LMGP, Grenoble, France for the high-temperature XRD measurements.

References

[1] J.F. Herbst, $R_2Fe_{14}B$ materials: Intrinsic properties and technological aspects, Rev. Mod. Phys. 63 (1991) 819. doi:https://doi.org/10.1103/RevModPhys.63.819.

[2] C.L. Chien, K.M. Unruh, Comparison of amorphous and crystalline FeB, Phys. Rev. B. 29 (1984) 207–211. doi:https://doi.org/10.1103/PhysRevB.29.207.

[3] T. Shigematsu, Mossbauer and Structural Studies on $(Fe_{1-x}Mn_x)_2B$, J. Phys. Soc. Japan. 39 (1975) 1233–1238. doi:10.1143/JPSJ.39.1233.

[4] C.L. Chien, D. Musser, E.M. Gyorgy, R.C. Sherwood, H.S. Chen, F.E. Luborsky, J.L. Walter, Magnetic properties of amorphous Fe_xB_{100-x} ($72 \leq x \leq 86$) and crystalline Fe_3B, Phys. Rev. B. 20 (1979). doi:https://doi.org/10.1103/PhysRevB.20.283.

[5] M. Kasaya, T. Hihara, Magnetic structure of MnB_2, J. Phys. Soc. Japan. 29 (1970). doi:https://doi.org/10.1143/JPSJ.29.336.

[6] K. Kádas, J. D Iuşan, J. Hellsvik, P. Cedervall, M. Berastegui, U. Sahlberg, Jansson, O. Eriksson, AlM_2B_2 (M = Cr, Mn, Fe, Co, Ni): a group of nanolaminated materials, J. Phys. Condens. Matter. 29 (2017) 155402. doi:10.1021/cm902023h.

[7] M. Ade, H. Hillebrecht, Ternary Borides Cr_2AlB_2 , Cr_3AlB_4 , and Cr_4AlB_6 : The First Members of the Series $(CrB_2)_nCrAl$ with n = 1, 2, 3 and a Unifying Concept for Ternary Borides as MAB-Phases, Inorg. Chem. 54 (2015) 6122–6135. doi:10.1021/acs.inorgchem.5b00049.

[8] P. Chai, S.A. Stoian, X. Tan, P.A. Dube, M. Shatruk, Investigation of magnetic properties and electronic structure of layered-structure borides AlT_2B_2 (T = Fe, Mn, Cr) and $AlFe_{2-x}Mn_xB_2$, J. Solid State Chem. 224 (2015) 52–61. doi:10.1016/j.jssc.2014.04.027.

[9] M. Elmassalami, D.D.S. Oliveira, H. Takeya, On the ferromagnetism of $AlFe_2B_2$, J. Magn. Magn. Mater. 323 (2011) 2133–2136. doi:10.1016/j.jmmm.2011.03.008.

[10] J. Cedervall, M.S. Andersson, T. Sarkar, E.K. Delczeg-Czirjak, L. Bergqvist, T.C. Hansen, P. Beran, P. Nordblad, M. Sahlberg, Magnetic structure of the magnetocaloric compound $AlFe_2B_2$, J. Alloys Compd. 664 (2016) 784–791. doi:10.1016/j.jallcom.2015.12.111.

[11] X. Tan, P. Chai, C.M. Thompson, M. Shatruk, Magnetocaloric effect in $AlFe_2B_2$: Toward magnetic refrigerants from earth-abundant elements, J. Am. Chem. Soc. 135 (2013) 9553–9557. doi:10.1021/ja404107p.

[12] Q. Du, G. Chen, W. Yang, J. Wei, M. Hua, H. Du, C. Wang, S. Liu, J. Han, Y. Zhang, J. Yang, Magnetic frustration and magnetocaloric effect in $AlFe_{2-x}Mn_xB_2$ (x = 0-0.5) ribbons, J. Phys. D. Appl. Phys. 48 (2015). doi:10.1088/0022-3727/48/33/335001.

[13] L. Ke, B.N. Harmon, M.J. Kramer, Electronic structure and magnetic properties in T_2AlB_2(T = Fe, Mn, Cr, Co, and Ni) and their alloys, Phys. Rev. B. 95 (2017) 104427. doi:10.1103/PhysRevB.95.104427.

[14] J. Rodríguez-Carvajal, Recent advances in magnetic structure determination by neutron powder diffraction, Phys. B Condens. Matter. 192 (1993) 55–69. doi:10.1016/0921-4526(93)90108-I.

[15] V. Petrícek, M. Dušek, L. Palatinus, Crystallographic computing system JANA2006: General features, Zeitschrift Fur Krist. 229 (2014) 345–352. doi:10.1515/zkri-2014-1737.

[16] L. Pauling, Crystal structure of hexagonal $MnAl_4$., Proc. Natl. Acad. Sci. U. S. A. 84 (1987) 3537–9. doi:10.1073/pnas.84.11.3537.

[17] A.D.I. Nicol, The structure of $MnAl_6$, Acta Crystallogr. 6 (1953) 285–293. doi:10.1107/S0365110X53000788.

[18] A.S. Cooper, Precise lattice constants of germanium, aluminum, gallium arsenide, uranium, sulphur, quartz and sapphire, Acta Crystallogr. 15 (1962) 578–582.

doi:10.1107/S0365110X62001474.

[19] V.H.J. Becher, K. Krogmann, E. Peisker, Uber das ternare Borid Mn_2AlB_2, Zeitschrift Fur Anorg. Und Allg. Chemie. (1966) 140–147.

[20] P.A. Joy, A. Kumar, S.K. Date, The relationship between field - cooled and zero - field - cooled susceptibilities of some ordered magnetic systems, J . Phys . Condens . Matter. 10 (1998) 11049–11054. doi:10.1088/0953-8984/10/48/024.

[21] L.H. Bennett, M. Rubinstein, G. Xiao, C.L. Chien, Magnetism and the observation of NMR lines in hexagonal Al_4Mn and icosahedral Al-Mn alloys, J. Appl. Phys. 61 (1987) 4364–4365. doi:10.1063/1.338422.

[22] H. Yasuoka, A. Soyama, K. Kimura, S. Takeuchi, NMR and Susceptibility Studies of $Al_{80}Mn_{20}$ Quasicrystal, J. Phys. Soc. Japan. 55 (1986) 1058–1061. doi:10.1143/JPSJ.55.1058.

[23] J. Hafner, M. Krajčí, Formation of magnetic moments in crystalline, quasicrystalline, and liquid Al-Mn alloys, Phys. Rev. B - Condens. Matter Mater. Phys. 57 (1998) 2849–2860. doi:10.1103/PhysRevB.57.2849.

[24] J.J. Hauser, H.S. Chen, J. V. Waszczak, Magnetic properties of Al-Si-Mn and Al-Mn quasicrystals and amorphous films, Phys. Rev. B. 33 (1986) 3577–3580. doi:10.1103/PhysRevB.33.3577.

[25] O. Rivin, E.N. Caspi, A. Pesach, H. Shaked, A. Hoser, R. Georgii, Q. Tao, J. Rosen, M.W. Barsoum, Evidence for ferromagnetic ordering in the MAX phase (Cr0.96Mn0.04)2GeC, Mater. Res. Lett. 5 (2017) 465–471. doi:10.1080/21663831.2017.1317295.

[26] W.K. Zhu, C.K. Lu, W. Tong, J.M. Wang, H.D. Zhou, S.X. Zhang, Strong ferromagnetism induced by canted antiferromagnetic order in double perovskite iridates $(La_{1-x}Sr_x)_2ZnIrO_6$, Phys. Rev. B - Condens. Matter Mater. Phys. 91 (2015) 1–8. doi:10.1103/PhysRevB.91.144408.

[27] F. Palacio, G. Antorrena, M. Castro, R. Burriel, J. Rawson, J.N.B. Smith, N. Bricklebank, J. Novoa, C. Ritter, High-temperature magnetic ordering in a new organic magnet, Phys. Rev. Lett. 79 (1997) 2336–2339. doi:10.1103/PhysRevLett.79.2336.

[28] H.J. Zeiger, G.W. Pratt, Magnetic interactions in solids, Clarendon Press, United Kingdom, 1973. doi:https://doi.org/10.1063/1.3128401.

[29] J. Rodriguez-Carvajal, BASIREPS: a program for calculating irreducible representations of space groups and basis functions for axial and polar vector properties, Solid State Phenom. 170 (2011) 263. doi:https://doi.org/10.4028/www.scientific.net/SSP.170.263.

Appendix A – Fitting procedure of field dependent magnetization data

M as a function of H_{ext} (Fig. 2(c)) includes three contributions (Eq. 1). The first, M_{sp}, originates from the FM component of the canted AFM structure of Mn_2AlB_2. Because we assume that the exchange interaction, which is responsible for this magnetic ordering, is significantly larger than $\mu_B H_{ext}$, M_{sp} is H_{ext} independent. The second term originates from a paramagnetic response of Mn in Mn_2AlB_2, induced by H_{ext}. Because these Mn ions are under the action of the exchange interaction, their paramagnetic response is assumed to be linear in H_{ext} [27,28]. The third term accounts for the paramagnetic contribution of the Mn ions within the impurities. Assuming that M is given in units of emu/g (Fig. 2(c)). The parameters to be determined within the (non-linear least squares) fit are M_{sp}, χ, n_i and S. We assume that the paramagnetic contribution of the (free) Mn ions within the impurities is that of Mn^{2+} (S=5/2) or Mn^{3+} (S=2) [28]. Hence, a valid result must yield S between 2 and 2.5. Taking into account this S range and the observed range of H_{ext} and T (Fig. 2(c)), B_S becomes linearly proportional to H_{ext} for 25 K < T. Hence, while χ, n_i and S are indistinguishable at this T range, their codependence with M_{sp} is very low. On the other hand, the derivation of M_{sp} for T < 25 K requires a multi-parameter (non-linear) fit process. To estimate the codependence between M_{sp} and χ, n_i, S we repeated the fit using the expected limits of S as well as a fitted S (Table A.II). Not only that the fitted S falls within the expected range, the variation in M_{sp} is small (~ 0.01 emu/g) and is added to the propagated statistical uncertainty in the 5 K M_{sp}. The 5 K parameters (Table A.II, first row) are then fixed within the fit process of the higher temperatures (Table A.I). Setting $\chi = 0$ and fixing S and n_i at their 5 K values not only leads to a worse fit agreement, but also leads to a significant deviation between the best fit and the observed M at higher temperatures.

Table A.I - The analyzed M_{sp} as a function of temperature, obtained by fitting Eq. 1 to the observed M (Fig. 2(c)) and varying M_{sp}, χ, n_i, and S.

T (K)	M_{sp} (emu/g)
5	0.28(2)
25	0.303(4)
50	0.303(3)
100	0.288(3)
200	0.269(1)
290	0.224(1)

Table A.II - The M_{sp}, S, n_i and χ derived using a non-linear fit of Eq. A1 to the observed M values at 5 K (Fig. 2(c)). In case a value was fixed during the fit process a (fix) symbol appears to its right.

M_{sp} (emu/g)	S	n_i	χ
0.28(6)	2(1)	0.02(2)	0.01(4)
0.29(1)	2 (fix)	0.025(2)	0.013(7)
0.26(1)	2.5 (fix)	0.018(1)	0.023(5)

Appendix B – Tables of XRD and NPD refined parameters

Table B.I: Refined LPs, the AFM Mn magnetic moments in μ_B, and the agreement factor R_f for the measured temperatures.

	T (K)	a (Å)	b (Å)	c (Å)	μ_{AFM} (μ_B)	R_f
HT XRD	308	2.92193(13)	11.0627(4)	2.90332(13)	+	2.53
	323	2.92217(15)	11.0599(5)	2.90597(15)	+	2.74
	373	2.92324(15)	11.0569(5)	2.91299(14)	+	2.81
	473	2.92629(12)	11.0584(4)	2.92534(12)	+	2.66
	573	2.92940(11)	11.0628(4)	2.93551(11)	+	2.57
	673	2.93275(10)	11.0702(3)	2.94438(10)	+	2.57
	773	2.93629(10)	11.0790(3)	2.95223(9)	+	2.57
RT XRD	298	2.92267(3)	11.0715(1)	2.89776(3)	+	8.8
NPD	1.6	2.9225(2)	11.0960(7)	2.8877(2)	0.71(2)	4.83
	5	2.9219(2)	11.0942(7)	2.8873(2)	0.69(2)	4.7
	10	2.9219(2)	11.0943(7)	2.8872(2)	0.69(2)	4.94
	25	2.9219(2)	11.0946(7)	2.8873(2)	0.68(2)	4.86
	50	2.9220(2)	11.0950(7)	2.8876(2)	0.69(2)	4.91
	65	2.9219(2)	11.0953(7)	2.8876(2)	0.69(2)	4.88
	100	2.9222(2)	11.0962(7)	2.8883(2)	0.68(2)	4.89
	200	2.9240(2)	11.0968(7)	2.8930(2)	0.64(2)	5.04
	298	2.9166(6)	11.048(3)	2.8930(6)	0.35(3)	5.06

+ Not considered

Table B.II: Temperature dependence of crystallographic, $R_{c,f}$, and magnetic $R_{m.f}$ agreement factors for two possible configurations, I and II (see text). Also listed, in last two columns, are the refined ordered magnetic moments (μ_{Mn}), assuming configurations, I and II.

T	$R_{c,f}$		$R_{m,f}$		μ_{AFM} (μ_B)	
(K)	I	II	I	II	I	II
1.6	5.15	4.83	27.9	23.1	0.70(2)	0.71(2)
5	4.79	4.7	27.7	23.6	0.67(2)	0.69(2)
10	5.02	4.94	27.5	23.4	0.67(2)	0.69(2)
25	4.95	4.86	27.8	24.2	0.66(2)	0.68(2)
50	5.08	4.91	27.7	23.5	0.67(2)	0.69(2)
65	5.17	4.88	27.4	22.9	0.67(2)	0.69(2)
100	4.95	4.89	28.9	23.9	0.66(2)	0.68(2)
200	5.1	5.04	30.1	25.5	0.63(2)	0.64(2)
298	5.04	5.06	48	47.1	0.35(2)	0.35(3)

- First time measurement of $Mn_2Al^{11}B_2$ using neutron powder diffraction
- $Mn_2Al^{11}B_2$ is determined to be an antiferromagnet at room temperature and below
- Magnetostriction is observed for the lattice parameters around room temperature
- Indications for a canted magnetic structure in $Mn_2Al^{11}B_2$ are found